SCHD
Structural & Congenital Heart Disease

Tech Science Press

http://doi.org/10.32604/schd.2026.077455

ARTICLE

Dynamic Plasma Exosomal miRNA Profiling Uncovers Molecular Trajectories of Cardiac Repair following Cone Reconstruction for Ebstein's Anomaly

Jiaxiong Wu[1,2,3,#], Runzhang Liang[1,#], Naijimuding ABUDUREXITI[4,#], Jing Ling[2], Zirui Peng[2], Jinxin Li[1], Canxin Wang[1], Yong Zhang[1], Haiyun Yuan[1,2,3,*] and Shusheng Wen[1,2,3,*]

[1]Department of Cardiac Surgery, Guangdong Provincial People's Hospital, Guangdong Academy of Medical Sciences, Southern Medical University, Guangzhou, China
[2]Department of Cardiac Surgery, Guangdong Cardiovascular Institute, Guangdong Provincial People's Hospital, Guangdong Academy of Medical Sciences, Guangzhou, China
[3]Guangdong Provincial Key Laboratory of South China Structural Heart Disease, Guangzhou, China
[4]Department of Cardiovascular Surgery, Guangdong Provincial Hospital of Chinese Medicine, The Second Affiliated Hospital of Guangzhou University of Chinese Medicine, Guangzhou, China
*Corresponding Authors: Haiyun Yuan. Email: yhy_yun@163.com; Shusheng Wen. Email: wenshusheng@gdph.org.cn
#These authors contributed equally to this work

Received: 09 December 2025; Accepted: 20 April 2026; Published: 11 June 2026

ABSTRACT: Objective: Cone reconstruction (CR) is the preferred surgical treatment for Ebstein's anomaly (EA). However, the molecular mechanisms underlying postoperative cardiac repair remain unclear. This study investigated the dynamic changes of plasma exosomal microRNAs (miRNAs) in EA patients before and after CR, exploring their association with postoperative cardiac function recovery and potential molecular mechanisms. **Methods:** Plasma samples were collected from 10 EA patients undergoing CR preoperatively, 1 day postoperatively, and 7 days postoperatively, along with samples from 10 healthy controls. Plasma exosomes were isolated using size-exclusion chromatography. Exosomal miRNAs were extracted and sequenced, followed by differential expression, functional enrichment, time-series clustering, and correlation analyses with clinical parameters. **Results:** Typical exosomes and miRNA profiles were identified. Preoperatively, EA patients exhibited distinct exosomal miRNA signatures enriched in pathways related to cardiac development, extracellular matrix remodeling, and apoptosis regulation. On postoperative day 1, miRNAs associated with inflammation and myocardial stress (miR-208a-3p, miR-208b-3p, and miR-499a-5p) were upregulated. By postoperative day 7, molecular pathways shifted toward structural remodeling and functional recovery, involving extracellular matrix organization and heart contraction regulation. Time-series clustering delineated an ordered molecular cascade associated with acute stress responses and structural remodeling. Five miRNAs persistently downregulated in the EA group were identified, potentially involved in key pathological processes including epigenetic regulation, metabolic processes, and muscle development. Notably, miR-224-5p, miR-548as-5p, and miR-30c-5p were significantly associated with right ventricular fractional area change, while miR-338-3p correlated with N-terminal pro-B-type natriuretic peptide dynamics. **Conclusion:** This study provides the first comprehensive dynamic landscape of plasma exosomal miRNAs in EA patients undergoing CR, with temporally coordinated molecular characteristics related to acute stress protection, structural remodeling, and functional recovery. Key miRNAs (miR-224-5p, miR-30c-5p, and miR-338-3p) may serve as potential molecular biomarkers and therapeutic targets for postoperative cardiac recovery, offering new insights into the molecular basis of CR-mediated cardiac repair in EA.

KEYWORDS: Congenital heart disease; Ebstein's anomaly; Cone reconstruction; exosomes; microRNAs

1 Introduction

Ebstein's anomaly (EA) is a rare congenital heart defect, with an estimated incidence of 1 to 5 per 200,000 live births, accounting for less than 1% of all congenital cardiac malformations [1,2]. It is characterized by abnormal tricuspid valve formation and right ventricular myopathy, leading to structural and functional impairments [3]. The main feature is apical displacement of the tricuspid valve leaflets, which may be accompanied by leaflet hypoplasia, downward displacement and dilation of the tricuspid annulus. The displaced leaflets cause right ventricular dilation and atrialization, thereby reducing effective right ventricular contractility [4]. Approximately 50% of EA cases are associated with other cardiac anomalies, such as atrial septal defect, patent foramen ovale, ventricular septal defect, pulmonary stenosis or atresia, and conduction system abnormalities [5,6].

The Cone reconstruction (CR) technique, introduced by Da Silva and colleagues in 2007 [7], is an improvement on the Carpentier technique. This method utilizes all available tricuspid valve tissue to reconstruct a cone-shaped valve, restoring central flow and leaflet coaptation, thereby approximating normal tricuspid anatomy and function. According to the 2025 Expert Consensus from the American Association for Thoracic Surgery, CR is beneficial when surgery is indicated, and is recommended as the preferred surgical approach for EA [8]. Compared with traditional repair techniques, this method is applicable to most anatomical variants of EA, demonstrates lower rates of tricuspid regurgitation recurrence, offers improved long-term valve durability, and favorably influences right ventricular remodeling [9,10].

Exosomes are a specific subtype of extracellular vesicles released from cells via the multivesicular body pathway [11]. They transport bioactive molecules such as proteins, nucleic acids, and metabolites between cells and tissues, and possess significant potential as biomarkers and therapeutic agents [12]. Exosome-mediated intercellular communication plays an important role in the pathogenesis and progression of cardiovascular diseases [13–15].

MicroRNAs (miRNAs) are small non-coding RNAs of approximately 22 nucleotides in length that regulate gene expression by binding to the 3′ untranslated region of target messenger RNAs (mRNAs), thereby reducing mRNA stability or inhibiting translation [16]. miRNAs are key regulators of gene expression [17,18], and dysregulation of miRNAs has been observed in various congenital heart diseases [19–21], including EA [22].

Despite the encouraging clinical results of CR, the underlying molecular and biological mechanisms contributing to postoperative cardiac recovery remain largely unexplored. This study aims to analyze the dynamic expression profiles of plasma exosomal miRNAs in EA patients before and after CR surgery and to explore the molecular mechanisms underlying postoperative cardiac repair.

2 Materials and Methods

2.1 Study Subjects

This study enrolled 10 patients with EA who underwent CR surgery at Guangdong Provincial People's Hospital between August 2023 and April 2025, forming the experimental group. The inclusion criteria were age 14 years or older; diagnosis of EA confirmed by preoperative transthoracic echocardiography; and an indication for surgical treatment with CR. The exclusion criteria were a history of prior cardiac surgery; the presence of other complex congenital heart malformations; acute decompensated heart failure; a history of or active infective endocarditis; impaired liver, kidney, or other organ function; perioperative blood transfusion; active rheumatic disease; and infectious diseases such as hepatitis B, hepatitis C, HIV, or syphilis.

2.2 Sample Collection

For the experimental group, 12 mL of venous blood was collected from each of the 10 patients at three time points: preoperatively, 1 day postoperatively, and 7 days postoperatively. All blood samples were collected into ethylenediaminetetraacetic acid blood collection tubes (367863, Becton Dickinson, Franklin Lakes, NJ, USA). For the control group, 12 mL of venous blood was collected from each of the 10 healthy individuals. Blood samples were either processed immediately or temporarily stored at 4°C and processed within 4 h. Samples were first centrifuged at 1500× *g* for 20 min at 4°C (centrifuge radius: 16.8 cm) to remove cellular components. The upper yellow plasma layer was carefully transferred to a new 15 mL centrifuge tube. The plasma was then centrifuged again at 3000× *g* for 15 min at 4°C (centrifuge radius: 16.8 cm) to remove residual blood cells. The supernatant plasma was carefully collected, aliquoted, and stored at −80°C. For clarity in data analysis and presentation, samples from the experimental group were labeled as "EA_Pre", "EA_Post1d", and "EA_Post7d", corresponding to preoperative, 1 day postoperative, and 7 days postoperative time points, respectively. Samples from the control group were labeled as "Control". The experimental workflow is depicted in Fig. 1.

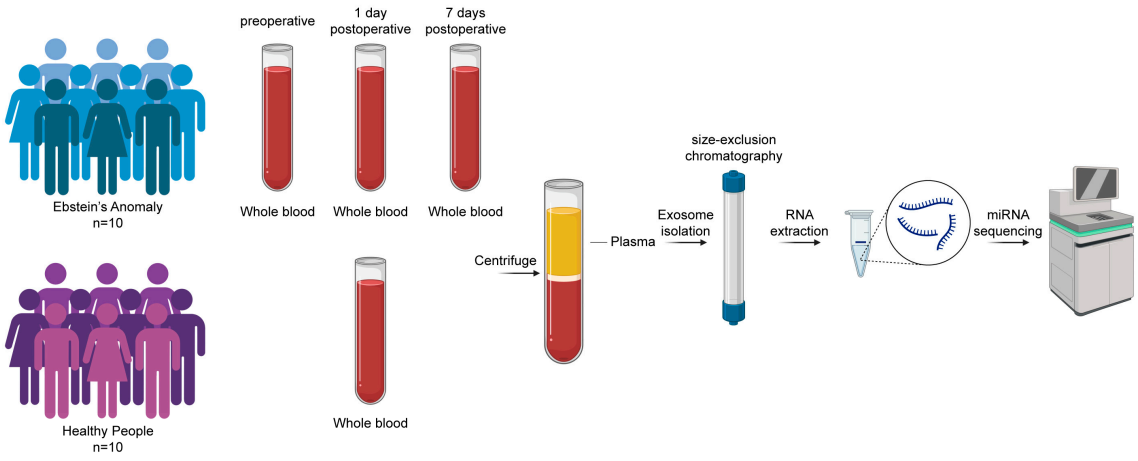

Figure 1: Experimental workflow.

2.3 Plasma Exosome Isolation

Exosomes were isolated by size-exclusion chromatography method according to the previously described approach [23]. Plasma samples were thawed and filtered through a 0.8 μm PES membrane (JT-PES-25, Jinteng, Tianjin, China), after which the filter was rinsed with PBS to obtain 1 mL of filtrate. Exosomes were isolated using Exosupur® SEC columns (ES9P14e, Echo Biotech, Beijing, China) according to the manufacturer's protocol. The columns were equilibrated with 10 mL of sterile PBS before sample loading. Each 1 mL plasma sample was applied to the column, and exosomes were eluted with PBS in 500 μL increments, collecting 2.5 mL of target fractions. The collected fractions were concentrated to approximately 200 μL using a 100 kDa Amicon® ultrafiltration tube (UFC810096, Merck Millipore, Germany) at 4000× *g* for 5–30 min at 4°C. For exosome characterization, the entire 200 μL was collected. For exosomal RNA extraction, 700 μL of lysis buffer was added to the concentrated sample and processed for downstream analysis.

2.4 Transmission Electron Microscopy

A 10 μL aliquot of the exosome solution was placed onto a copper grid and incubated at room temperature for 10 min. The grid was then rinsed with sterile distilled water, and excess liquid was removed using filter paper. Next, 10 μL of 2% uranyl acetate was applied to the grid for negative staining (1 min). Excess stain was removed with filter paper, and the grid was air-dried under an incandescent lamp for 2 min. The prepared grid was examined under a transmission electron microscope (H-7650, Hitachi Ltd., Tokyo, Japan) at an accelerating voltage of 80 kV to capture images of exosome morphology and size.

2.5 Western Blot Analysis

Exosome protein concentrations were quantified using the Pierce BCA Protein Assay Kit (23227, Thermo Fisher Scientific, Rockford, IL, USA). The exosome supernatants were mixed with 5 × sodium dodecyl sulfate loading buffer and boiled for denaturation before western blot analysis. A 10% sodium dodecyl sulfate-polyacrylamide gel was used for electrophoresis. 20 μg of protein was loaded in each lane. Proteins were transferred to 0.2 μm polyvinylidene fluoride membranes (ISEQ00010, Merck Millipore, Tullagreen, Co. Cork, Ireland) using an eBlot L1 Fast Wet Transfer System (L00686C, GenScript Biotech, Nanjing, China). The membranes were then blocked with 5% skim milk powder. After blocking, the membranes were incubated with primary and secondary antibodies according to the manufacturer's protocols. Membranes were treated with the ECL Western Blotting Substrate (PE0010, Solarbio, Beijing, China) and visualized using an automatic chemiluminescence imaging system (Tanon-5200Multi, Tanon, Shanghai, China). The primary antibodies used in this study were rabbit monoclonal antibodies against TSG101 (ab125011, Abcam, USA, 0.222 mg/mL), Alix (ab186429, Abcam, USA, 1.244 mg/mL), CD9 (ab263019, Abcam, USA, 0.531 mg/mL), HSP70 (ab181606, Abcam, USA, 1.17 mg/mL), and rabbit polyclonal antibody Calnexin (10427-2-AP, Proteintech, Chicago, IL, USA, 0.55 mg/mL). The secondary antibody was the HRP-conjugated Goat Anti-Rabbit IgG (SA00001-2, Proteintech, Chicago, IL, USA, 0.2 mg/mL).

2.6 Nanoparticle Tracking Analysis

The particle size distribution and concentration of exosomes were measured using a Flow NanoAnalyzer (N30E, NanoFCM Inc., Xiamen, China). Samples were first diluted with PBS to an estimated particle concentration of 10^8 particles/mL for measurement. The instrument flow rate was determined by counting fluorescent silica nanospheres (250 nm) of known concentration passing through the detection system within a defined period. Under the same injection pressure, the particle counts obtained from the sample were used to calculate its particle concentration. For particle size distribution, a calibration curve correlating scattering intensity with particle diameter was generated using silica standard beads (68 nm, 91 nm, 113 nm, and 155 nm).

2.7 Total RNA Extraction

Total RNA was extracted from plasma exosomes using the Exosome RNA Purification Kit (5202050, Simgen, Hangzhou, China) following the manufacturer's instructions. 100 μL of exosome solution was lysed with 700 μL of Buffer TL to release and stabilize RNA. The sample was then mixed with 10 μL of Buffer EX and centrifuged to precipitate proteins. The supernatant was combined with absolute ethanol and loaded onto a nucleic acid purification column. After sequential washing with Buffers WA and WBR, RNA was eluted with 35 μL of RNase-free water.

2.8 miRNA Library Preparation and Sequencing

Small RNA libraries were constructed using the QIAseq miRNA Library Kit (Qiagen, Frederick, MD, USA) according to the manufacturer's instructions. Briefly, total RNA was used as the input for library preparation. In an unbiased ligation reaction, specially designed 3′ and 5′ adapters were sequentially ligated to mature miRNAs on ice. The ligated miRNAs were then reverse transcribed into complementary DNA using a reverse transcription primer containing an integrated unique molecular identifier. Following complementary DNA clean-up with QIAseq miRNA NGS Beads, library amplification was performed by polymerase chain reaction with a universal forward primer and indexing reverse primers. Library quality was assessed by analyzing 1 μL of each miRNA library using a High Sensitivity DNA Kit (5067-4626, Agilent Technologies, Santa Clara, CA, USA) on an Agilent 2100 Bioanalyzer (G2939B, Agilent Technologies, Santa Clara, CA, USA) following the manufacturer's instructions. Libraries that passed quality control were subjected to paired-end sequencing on the Illumina NovaSeq platform to generate raw sequencing data.

2.9 Alignment to Reference Genome and miRNA Identification

Clean reads were aligned with the Silva, GtRNAdb, Rfam, and Repbase databases using Bowtie software to filter out repetitive sequences and non-coding RNAs, such as ribosomal RNA, transfer RNA, small nuclear RNA, and small nucleolar RNA, resulting in unannotated reads containing miRNAs. The unannotated reads were then aligned to the human reference genome GRCh38 using Bowtie to obtain their genomic locations, referred to as mapped reads. Known miRNAs were identified and novel miRNAs were predicted using the integrated miRDeep2 software package.

2.10 miRNA Expression Quantification and Differential Expression Analysis

The expression level of each miRNA in a sample was calculated using the formula: $TPM = \frac{\text{ReadCount} \times 1{,}000{,}000}{\text{MappedReads}}$, where ReadCount represents the number of reads mapped to a specific miRNA, and MappedReads represents the total number of reads mapped to all miRNAs. Reads with the same unique molecular identifier were counted as single reads. Differential expression analysis between two groups was performed using the edgeR R package (version 3.12.1). edgeR employs a Poisson distribution model and empirical Bayes methods to identify statistically significant differences in digital miRNA expression data. To control the false discovery rate, p-values were adjusted using the Benjamini-Hochberg method. miRNAs with $\left|\log_2(Fold\ Change)\right| \geq 1.5$ and an edgeR-adjusted p-value ≤ 0.05 were considered differentially expressed.

2.11 Target Gene Functional Annotation

The target genes of differentially expressed miRNAs (DEMs) were predicted using miRanda [24] and RNAhybrid [25]. Functional annotation of target genes was performed using BLAST software against Nr (NCBI non-redundant protein sequences), Pfam (Protein family), KOG/COG (Clusters of Orthologous Groups of proteins), Swiss-Prot (A manually annotated and reviewed protein sequence database), KEGG (Kyoto Encyclopedia of Genes and Genomes), and GO (Gene Ontology) databases.

2.12 Functional Enrichment Analysis

Gene Ontology (GO) enrichment analysis of differentially expressed genes was performed using the topGO R package (version 2.18.0). Kyoto Encyclopedia of Genes and Genomes (KEGG) pathway enrichment analysis was performed using the KOBAS software.

2.13 Statistical Analysis

All statistical analyses were performed using R software (version 4.2.1). Correlations were assessed using Spearman's rank correlation coefficient. Group comparisons were conducted using the Student's *t*-test, while categorical variables were analyzed with Fisher's exact test. All statistical tests were two-tailed, and a p-value ≤ 0.05 was considered statistically significant.

3 Results

3.1 Population Characteristics

A total of 10 patients were included in the experimental group, with a median age of 40.5 years (interquartile range [IQR] 32.0–49.0) and a composition of 4 male and 6 female patients. Eight patients (80.0%) were in New York Heart Association (NYHA) class II and 2 (20.0%) in class III. According to Carpentier's classification, 2 (20.0%), 4 (40.0%), and 4 (40.0%) patients were classified as type A, B, and C, respectively. Many patients presented with severe tricuspid regurgitation (9 patients, 90.0%), while only 1 (10.0%) had moderate regurgitation. The median right ventricular fractional area change (RV-FAC) was 40.5% (IQR 39.5%–43.5%), and the median cardiothoracic ratio was 0.6 (IQR 0.5–0.7), see Table 1.

Table 1: Baseline characteristics of the experimental group.

Parameters	Values
Age (y)	40.5 (32.0, 49.0)
Body mass index (kg/m^2)	21.2 (20.2, 26.2)
Sex (Male/Female)	4/6
NYHA class	
NYHA II	8 (80.0%)
NYHA III	2 (20.0%)
SpO_2 (%)	99.0 (96.0, 100.0)
Carpentier's classification	
A	2 (20.0%)
B	4 (40.0%)
C	4 (40.0%)
Tricuspid regurgitation severity	
Moderate	1 (10.0%)
Severe	9 (90.0%)
RV-FAC (%)	40.5 (39.5, 43.5)
Cardiothoracic ratio	0.6 (0.5, 0.7)
Surgical time (min)	223.5 (193.0, 280.0)
CPB time (min)	117.0 (107.0, 141.0)
ACC time (min)	73.5 (64.0, 79.0)
ICU length of stay (d)	2.0 (1.8, 4.1)
Mechanical ventilation duration (h)	15.7 (6.0, 20.8)
Post-ICU hospital stays (d)	6.0 (5.0, 7.9)

*Note: Values are presented as median (interquartile range) for continuous variables and frequency (percentage) for categorical variables. NYHA, New York Heart Association; SpO_2, peripheral oxygen saturation; RV-FAC, right ventricular fractional area change; CPB, cardiopulmonary bypass; ACC, aortic cross-clamp; ICU, intensive care unit.

3.2 Characterization of Plasma Exosomes

Nanoparticle tracking analysis revealed that the particle size distribution peaked at approximately 67.25 nm, with an average diameter of 73.51 nm (Fig. 2A). Transmission electron microscopy showed exosomes with the typical cup-shaped morphology and intact membranes, consistent with the characteristic structure of exosomes (Fig. 2B). Western blot analysis confirmed the presence of the exosomal marker

proteins TSG101, Alix, CD9, and HSP70, while the negative marker Calnexin was absent (Fig. 2C). Collectively, these results indicate that high-purity plasma exosomes were successfully isolated using size-exclusion chromatography.

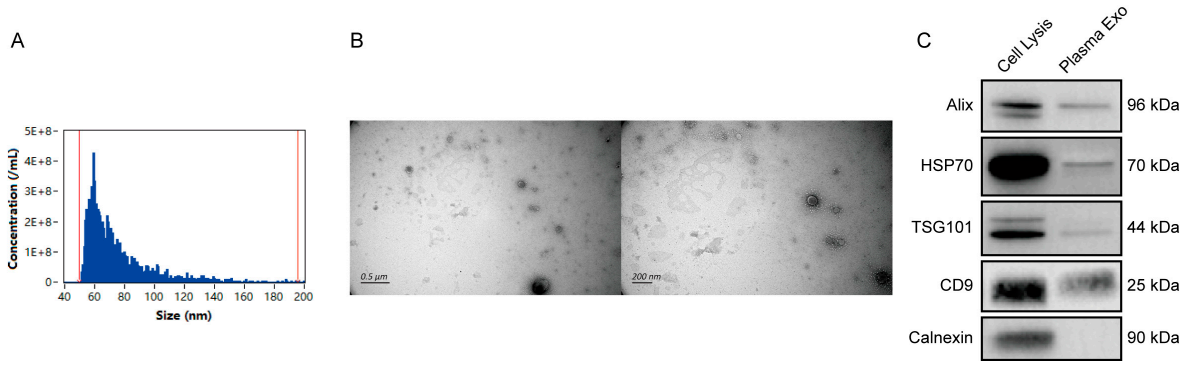

Figure 2: Identification of plasma exosomes. (**A**) Particle size distribution analysis of exosomes by nanoparticle tracking analysis. (**B**) Representative morphological structures of exosomes observed by transmission electron microscopy (scale bars: 0.5 μm and 200 nm). (**C**) Western blot analysis detecting the expression of TSG101, Alix, CD9, HSP70, and Calnexin in exosomes.

3.3 Differential Expression of Exosomal miRNAs in EA Patients Undergoing CR

Quality control of sequencing data demonstrated high data integrity across all samples. A total of 1056 miRNAs were predicted, including 975 known miRNAs and 81 novel miRNAs.

Compared with the Control group, the EA_Pre group exhibited 26 DEMs (8 upregulated and 18 downregulated). Notably, cardioprotective miRNAs such as miR-222-3p and miR-150-5p were significantly downregulated [26,27] (Fig. 3A,B).

When comparing EA_Pre with EA_Post1d, 22 miRNAs showed differential expression (20 upregulated and 2 downregulated). Among them, miR-223-3p, known to suppress cardiac inflammation and apoptosis, was markedly upregulated [28]. Several cardiac-enriched or cardiac-specific miRNAs, including miR-208a-3p, miR-208b-3p, and miR-499a-5p, also exhibited sharp increases in expression. These miRNAs are well-recognized regulators of myocardial injury and stress [29,30], and their significant upregulation strongly suggests cardiomyocyte damage induced by surgery and the rapid activation of early repair mechanisms, highlighting their potential as acute-phase biomarkers following cardiac surgery (Fig. 3C,D).

Comparison between the EA_Pre and EA_Post7d groups revealed 38 DEMs (30 upregulated and 8 downregulated). Interestingly, several miRNAs that were upregulated at postoperative day 1 (such as miR-16-2-3p, miR-208a-3p, miR-208b-3p, and miR-499a-5p) showed a trend toward baseline levels, whereas new miRNAs such as miR-148a-3p, which promotes cardiac reprogramming and improves heart function [31], began to display differential expression, suggesting the activation of repair and remodeling mechanisms (Fig. 3E,F).

3.4 Functional Enrichment Analysis of DEMs Reveals Dynamic Biological Processes and Pathways

To gain deeper insight into the core pathological mechanisms of EA and the repair process following CR, this study focused on GO biological processes and KEGG pathways closely related to cardiac development, structural remodeling, cell survival, and functional recovery. Enrichment analysis of DEMs allowed us to construct a disease-specific molecular profile and delineate dynamic regulatory pathways from acute protective responses to subacute repair following surgery (Fig. 4).

Differential miRNAs between the Control and EA_Pre groups were primarily enriched in biological processes associated with cardiac development, myocardial structure, and functional regulation. GO biological process analysis revealed significant enrichment in terms such as negative regulation of apoptotic process, cardiac muscle tissue growth, Notch signaling involved in heart development, cardiac ventricle morphogenesis, and regulation of extracellular matrix disassembly (Fig. 4A), indicating that EA patients exhibit preoperative abnormalities in cardiomyocyte apoptosis, ventricular morphogenesis, and extracellular matrix remodeling. KEGG pathway analysis further showed that these miRNAs were mainly involved in Protein digestion and absorption, Chemokine signaling pathway, Adrenergic signaling in cardiomyocytes, Vascular smooth muscle contraction, and Leukocyte transendothelial migration (Fig. 4B), reflecting preoperative dysregulation in myocardial metabolism, neurohormonal regulation, and inflammatory responses.

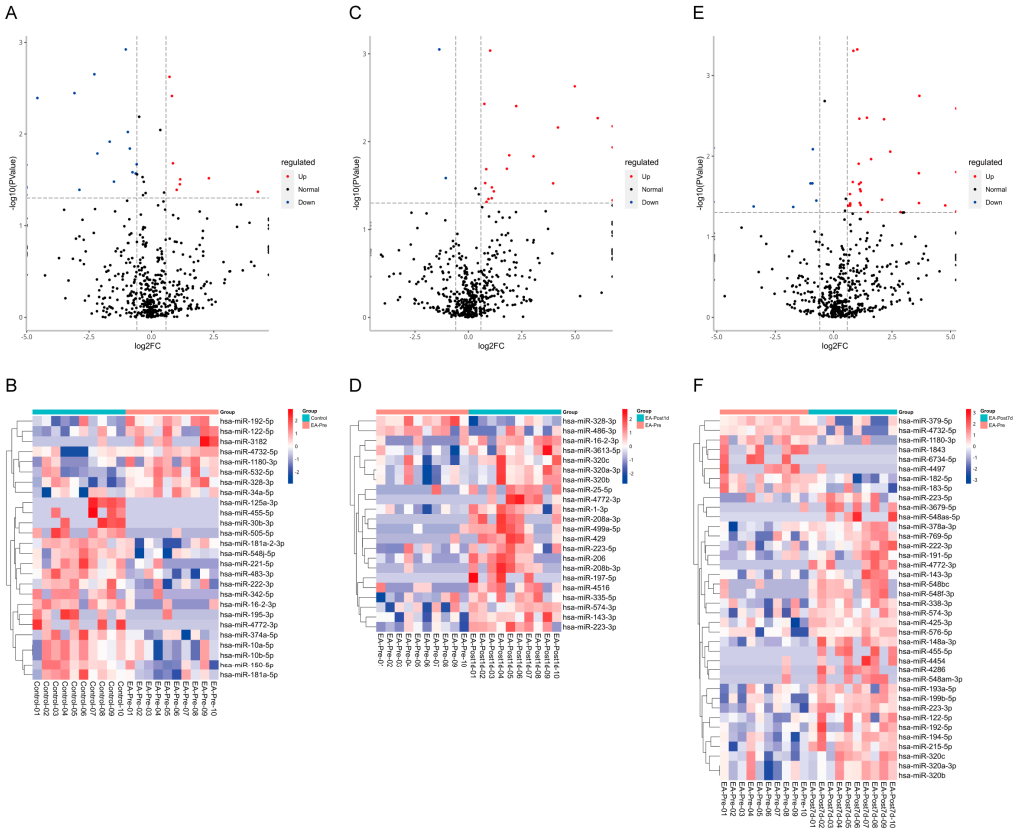

Figure 3: Dynamic changes of exosomal miRNA profiles in EA patients undergoing CR surgery. Upper panel: Volcano plots illustrating DEMs. (**A**) Control vs. EA_Pre. (**C**) EA_Pre vs. EA_Post1d. (**E**) EA_Pre vs. EA_Post7d. In all volcano plots (**A**,**C**,**E**), red points represent significantly upregulated miRNAs, blue points represent significantly downregulated miRNAs (adjusted p-value ≤ 0.05 and $\left|\log_2(Fold\ Change)\right| \geq 1.5$), and gray points are non-significant. Lower panel: Hierarchical clustering heatmaps of the DEMs identified in the corresponding volcano plots. (**B**) Control vs. EA_Pre. (**D**) EA_Pre vs. EA_Post1d. (**F**) EA_Pre vs. EA_Post7d. In all heatmaps (**B**,**D**,**F**), each row represents a miRNA, and each column represents an individual sample. The color bar on top indicates the sample groups. Expression levels are z-score normalized per row, with red indicating high expression and blue indicating low expression. EA, Ebstein's anomaly; CR, Cone reconstruction; DEMs, differentially expressed miRNAs.

Comparison of EA_Pre with EA_Post1d revealed that DEMs were significantly enriched in biological processes related to angiogenesis, anti-apoptosis, and hypoxia response. GO analysis highlighted enrichment in positive regulation of angiogenesis, cellular response to hypoxia, negative regulation of endothelial cell apoptotic process, ERK1 and ERK2 cascade, and Notch signaling pathway (Fig. 4C), suggesting early postoperative activation of vascular growth and cell survival signaling pathways. KEGG analysis indicated that these miRNAs were primarily involved in pathways such as VEGF signaling pathway, PI3K-Akt signaling pathway, Focal adhesion, MAPK signaling pathway, and HIF-1 signaling pathway (Fig. 4D), which are closely associated with cell proliferation, survival, and metabolic regulation, demonstrating tissue repair and adaptive responses in the early postoperative phase.

For the EA_Pre vs. EA_Post7d comparison, the functional enrichment of DEMs shifted toward tissue structural remodeling and immune regulation. GO analysis showed significant enrichment in terms such as extracellular matrix organization, positive regulation of angiogenesis, regulation of cell cycle, regulation of heart contraction, and regulation of aerobic respiration (Fig. 4E), indicating that the heart had entered a repair phase, with active structural reconstruction and metabolic adjustment. KEGG pathway analysis further revealed significant enrichment in pathways including Notch signaling pathway, phagosome, cell adhesion molecules (CAMs), antigen processing and presentation, and inflammatory bowel disease (IBD) (Fig. 4F), reflecting molecular features of mid-term immune regulation and myocardial structural remodeling following surgery.

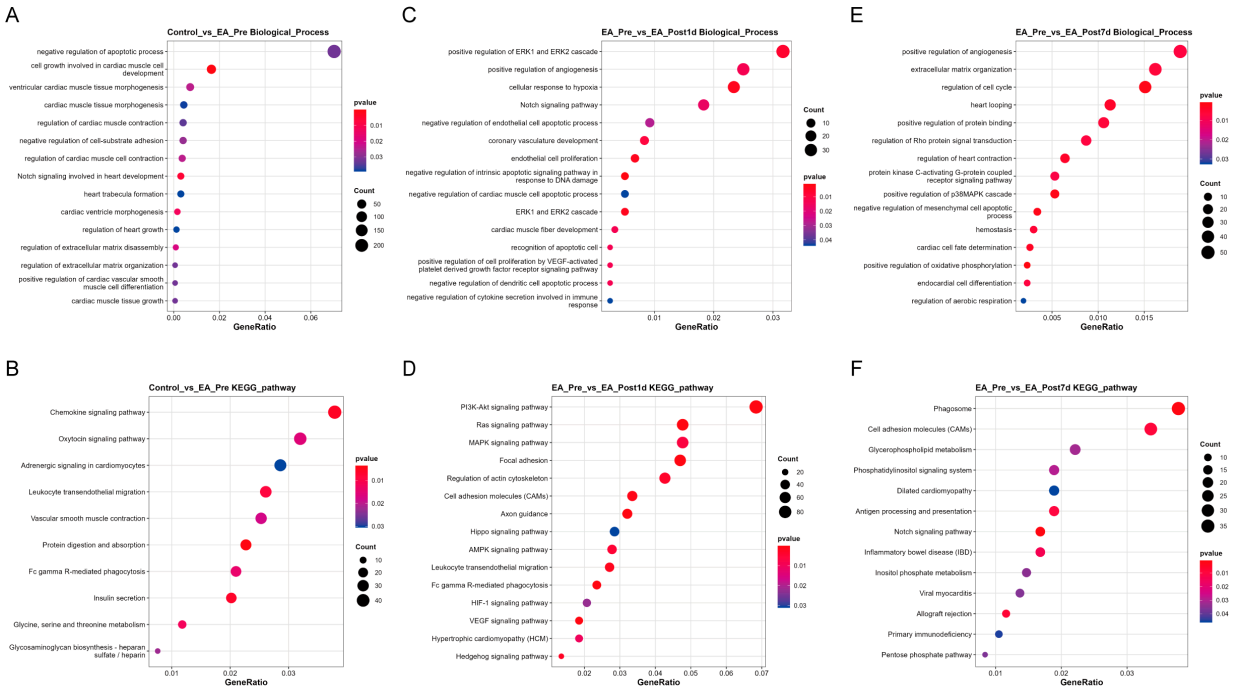

Figure 4: Functional enrichment analysis of predicted target genes for DEMs. Bubble plots display the significantly enriched GO Biological Process terms (**A**,**C**,**E**) and KEGG pathways (**B**,**D**,**F**) for the three comparison groups: (**A**,**B**) Control vs. EA_Pre, (**C**,**D**) EA_Pre vs. EA_Post1d, and (**E**,**F**) EA_Pre vs. EA_Post7d. The *x*-axis represents the GeneRatio. Bubble color and size represent the statistical significance and the number of genes enriched in the term, respectively. DEMs, differentially expressed miRNAs; GO, Gene Ontology; KEGG, Kyoto Encyclopedia of Genes and Genomes.

3.5 Identification of Core miRNAs and Their Functional Landscape in EA

We compared the differentially expressed exosomal miRNAs among Control vs. EA_Pre, Control vs. EA_Post1d, and Control vs. EA_Post7d groups to further elucidate the miRNA regulatory landscape of EA. A Venn diagram analysis identified five common DEMs shared across all three comparisons (Fig. 5A): miR-181a-2-3p, miR-181a-5p, miR-221-5p, miR-342-5p, and miR-483-3p. All five miRNAs were downregulated in EA patients preoperatively and postoperatively (1 day and 7 days) compared to healthy controls, suggesting their potential involvement in the core pathophysiological mechanisms of EA.

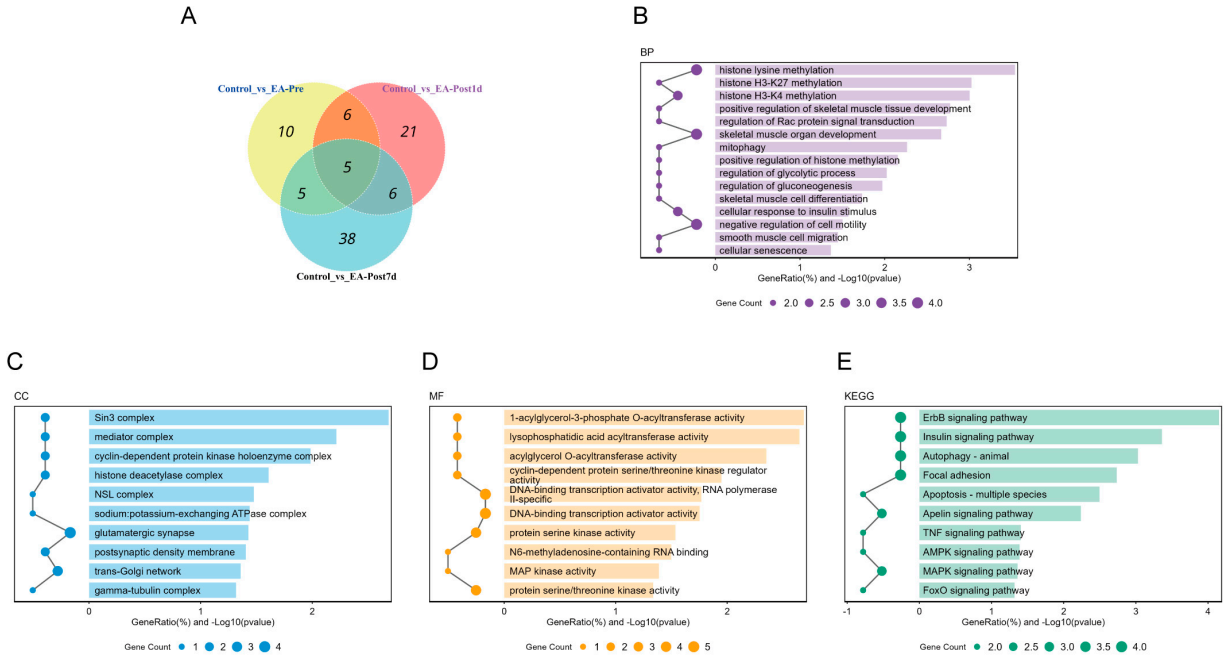

Figure 5: Identification of core downregulated miRNAs and functional enrichment analysis of their target genes. (**A**) Venn diagram. The diagram illustrates the overlap of DEMs across the three comparisons: Control vs. EA_Pre, Control vs. EA_Post1d, and Control vs. EA_Post7d. (**B**–**D**) GO enrichment analysis for the target genes of the five core miRNAs, showing the significantly enriched terms in (**B**) biological process, (**C**) cellular component, and (**D**) molecular function categories. (**E**) KEGG pathway enrichment analysis for the target genes. For panels B-E, the length of the bar represents the statistical significance. The position of the dot along the negative *x*-axis indicates the GeneRatio, and the dot size is proportional to the number of genes enriched in the term. Term descriptions are displayed to the left of the bars. DEMs, differentially expressed miRNAs; GO, Gene Ontology; BP: biological process; CC: cellular component; MF: molecular function; KEGG, Kyoto Encyclopedia of Genes and Genomes.

Functional enrichment of the predicted target genes of these five miRNAs provided further insights. GO biological process analysis revealed significant enrichment in categories related to epigenetic regulation, such as histone lysine methylation, histone H3-K27 methylation, and histone H3-K4 methylation; muscle development, including positive regulation of skeletal muscle tissue development and skeletal muscle organ development; and mitophagy and metabolic regulation, such as mitophagy and regulation of glycolytic process (Fig. 5B).

GO cellular component analysis indicated that the target genes were mainly associated with transcriptional regulatory complexes, including the Sin3 complex and mediator complex, as well as

with cyclin-dependent protein kinase holoenzyme complex, histone deacetylase complex, sodium: potassium-exchanging ATPase complex, glutamatergic synapse, and trans-Golgi network (Fig. 5C).

GO molecular function analysis showed significant enrichment in categories related to lipid metabolism, such as 1-acylglycerol-3-phosphate O-acyltransferase activity and acylglycerol O-acyltransferase activity, protein phosphorylation and signaling, including protein serine kinase activity and protein serine/threonine kinase activity, and transcriptional regulation, such as DNA-binding transcription activator activity, RNA polymerase II-specific. Additionally, MAP kinase activity was also among the enriched functions (Fig. 5D).

KEGG pathway enrichment analysis demonstrated that the target genes of these five miRNAs were significantly involved in pathways related to cardiac structure, stress response, and energy metabolism, with the ErbB signaling pathway, Insulin signaling pathway, Autophagy-animal, and Focal adhesion ranking among the most prominent (Fig. 5E).

Collectively, these results indicate that the five persistently downregulated miRNAs may play crucial roles in the pathogenesis and progression of EA by coordinately regulating epigenetic modification, muscle development, metabolic processes, and key signaling pathways.

3.6 ROC Curve Analysis of DEMs

Based on all DEMs identified in the Control vs. EA_Pre comparison, we extracted their expression data to generate receiver operating characteristic (ROC) curves and calculate the area under the curve (AUC). Leave-one-out cross-validation (LOOCV) was employed to mitigate potential evaluation bias associated with the limited sample size. Analysis of the five common DEMs showed that the AUC values for miR-181a-2-3p, miR-181a-5p, miR-221-5p, miR-342-5p, and miR-483-3p were 0.71, 0.75, 0.70, 0.62, and 0.85, respectively (Fig. 6A). Furthermore, we applied logistic regression to construct a multi-miRNA classifier. The LOOCV method demonstrated that a four-miRNA panel (miR-483-3p, miR-192-5p, miR-532-5p, and miR-16-2-3p) achieved markedly superior discriminatory performance compared with any single miRNA, with an AUC as high as 0.99 (Fig. 6B).

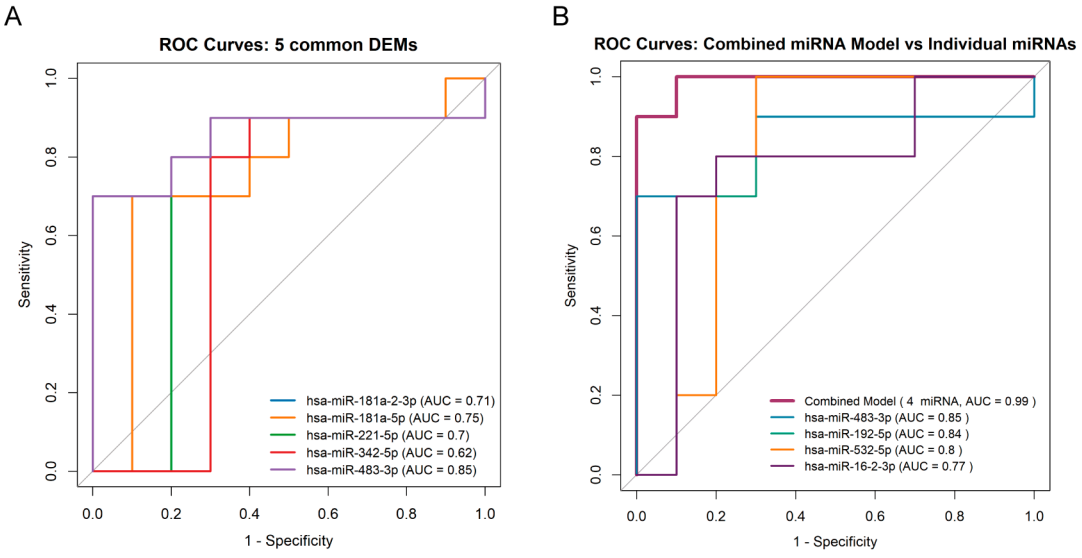

Figure 6: The receiver operating characteristic (ROC) analysis of DEMs. Different colored curves represent different miRNAs. AUC denotes the area under the curve. (**A**) Five common DEMs. (**B**) Combined miRNA model and individual miRNAs. DEMs, differentially expressed miRNAs.

3.7 Temporal Clustering of miRNAs Reveals Dynamic Molecular Cascade

A time-series clustering analysis of DEMs was performed to further explore the temporal regulatory landscape of exosomal miRNAs following CR and identified five distinct miRNA clusters (C1–C5). The combined expression dynamics and functional enrichment analyses delineate a molecular cascade associated with acute adaptation and structural remodeling (Fig. 7). The cluster assignment for each miRNA is provided in the Supplementary Table S1.

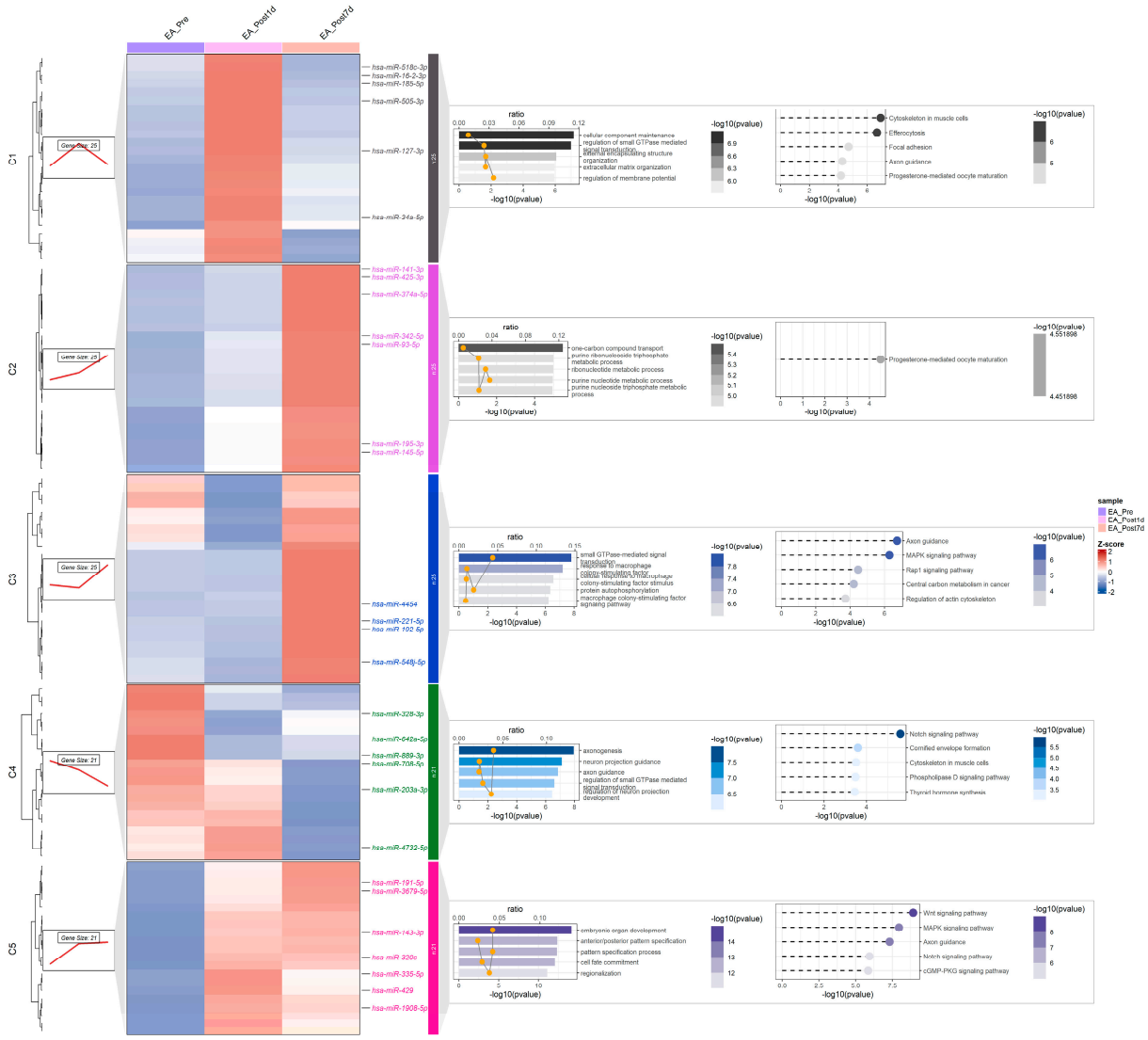

Figure 7: Temporal clustering and functional enrichment of DEMs. Time-series clustering of miRNAs was performed using the ClusterGVis software package. Left panel: Line plots illustrate the expression trends of miRNAs within each cluster (C1–C5) across the three time points (EA_Pre, EA_Post1d, EA_Post7d). The cluster serial number and the number of miRNAs contained within each cluster (cluster size) are indicated. Middle panel: Heatmaps display the normalized expression levels of miRNAs in each cluster across all individual samples grouped by time point. Right panel: The most significantly enriched GO Biological Process terms and KEGG pathways for the target genes of miRNAs in each cluster are displayed. DEMs, differentially expressed miRNAs; GO, Gene Ontology; KEGG, Kyoto Encyclopedia of Genes and Genomes.

Cluster C1 target genes were significantly enriched in cellular component maintenance, extracellular matrix organization, and regulation of membrane potential. KEGG pathway analysis further implicated Cytoskeleton in muscle cells, Efferocytosis, and Focal adhesion. These findings suggest that C1 miRNAs may regulate myocardial structural integrity, tissue repair, and inflammatory resolution during the acute postoperative phase, serving as an early adaptive response to surgical stress and direct tissue injury.

Cluster C2 showed strong enrichment in metabolic processes such as purine ribonucleoside triphosphate metabolic processes and purine nucleotide metabolic processes. This indicates that cellular energy metabolism and nucleotide biosynthesis were markedly activated in the early postoperative period, potentially providing the bioenergetic and biosynthetic support necessary for cell proliferation and tissue regeneration.

Cluster C3 was characterized by enrichment in small GTPase-mediated signal transduction and response to macrophage colony-stimulating factor, with KEGG pathways notably involving MAPK signaling pathway and Rap1 signaling pathway. These results strongly suggest that C3 miRNAs participate in key intracellular signaling networks and immune regulatory processes, thereby playing a central role in initiating tissue repair and inflammatory resolution.

Cluster C4 target genes were enriched in neuron-related processes such as axonogenesis and neuron projection guidance, alongside the Notch signaling pathway and Cytoskeleton in muscle cells in KEGG analysis. Emerging evidence links congenital heart disease with neurological and cognitive impairments, yet the underlying molecular connections remain poorly defined. These findings suggest that C4 miRNAs might be involved in neuro-cardiac interactions during postoperative recovery.

Cluster C5 exhibited the most prominent enrichment signatures, with target genes involved in embryonic organ development, anterior/posterior pattern specification, and cell fate commitment. KEGG pathway analysis further highlighted Wnt signaling pathway, MAPK signaling pathway, and Notch signaling pathway. These results strongly indicate that CR surgery may reactivate developmental molecular programs that are essential during embryonic heart formation, contributing to postoperative structural remodeling and functional restoration of the heart.

Collectively, these time-series clustering results reveal that postoperative cardiac recovery is governed by a dynamic, multi-phase miRNA regulatory network, associated with acute repair and metabolic activation (C1–C3) and neuro-cardiac communication and developmental reprogramming (C4–C5), suggesting a coordinated molecular response of the myocardium following CR of EA.

3.8 Correlation Between Postoperative miRNA Dynamics and Cardiac Functional Recovery

Correlation analysis between the 7-day postoperative changes in DEMs ($\log_2$FC) and echocardiographic parameters (Table 2) was performed to explore their relationship with acute cardiac functional recovery. The results revealed that three miRNAs were significantly correlated with the change in RV-FAC ($|r| > 0.5$, p-value ≤ 0.05). Among them, miR-224-5p showed the strongest correlation with RV-FAC change ($r = -0.874$, p-value = 0.0045) after FDR correction, suggesting its potential role as a key regulatory factor in early postoperative cardiac functional recovery.

Table 2: Key miRNAs correlated with acute postoperative changes in RV-FAC.

miRNA	Correlation Coefficient (r)	p-value	$\log_2$FC
miR-224-5p	−0.874	0.0045	1.41
miR-548as-5p	−0.752	0.0314	1.58
miR-30c-5p	−0.749	0.0324	0.68

Further analysis revealed that postoperative changes in miRNA expression at day 7 were also significantly associated with mid-term (3-month) changes in RV-FAC (Table 3) after FDR correction. Four miRNAs exhibited significant correlations with 3-month RV-FAC changes, among which miR-224-5p, miR-548as-5p, and miR-30c-5p consistently correlated with both acute and mid-term cardiac functional recovery, indicating their potential as stable biomarkers of the postoperative remodeling trajectory.

Table 3: Key miRNAs correlated with mid-term postoperative changes in RV-FAC.

miRNA	Correlation Coefficient (r)	*p*-value	$\log_2$FC
miR-224-5p	−0.870	0.0050	1.41
miR-548as-5p	−0.866	0.0055	1.58
miR-548bc	0.795	0.0182	3.81
miR-30c-5p	−0.711	0.0478	0.68

In addition, we explored the associations between miRNA expression and the heart failure biomarker N-terminal pro-B-type natriuretic peptide (NT-proBNP). Preoperative NT-proBNP levels were correlated with the expression of several miRNAs at baseline. Notably, miR-338-3p was not only significantly correlated with NT-proBNP levels preoperatively, but its postoperative expression changes were also associated with alterations in NT-proBNP levels (Tables S2 and S3). This consistent association across static and dynamic analyses highlights the potential role of miR-338-3p as a sensitive indicator of myocardial stress.

4 Discussion

Through longitudinal analysis of plasma exosomal miRNA expression profiles in patients with EA undergoing CR, this study is the first to systematically delineate the dynamic molecular landscape underlying both the disease state and the postoperative cardiac repair process. Preoperatively, EA patients displayed a distinct exosomal miRNA signature. Postoperatively, CR triggered a transition from acute stress and protective mechanisms on day 1 to structural remodeling and functional recovery by day 7. Furthermore, we identified a group of persistently dysregulated miRNAs in the EA group, which may contribute to the core pathophysiological mechanisms of EA. Another group of key miRNAs demonstrated significant correlations with postoperative functional recovery. Collectively, these findings provide novel insights into the molecular basis of cardiac remodeling and recovery following CR and offer a new perspective for understanding the underlying pathophysiology of EA.

Our findings are consistent with recent studies on exosome-mediated cardiac repair, in which exosomes and their cargo miRNAs have been widely reported to regulate cardiomyocyte survival, inflammation, angiogenesis, and fibrosis, serving as crucial mediators of intercellular communication following cardiac injury [32,33]. In our study, the marked upregulation of miRNAs related to inflammation and injury observed on postoperative day 1 likely reflects transient myocardial stress, ischemia-reperfusion injury, and inflammatory activation during the perioperative period. By postoperative day 7, however, the miRNA expression signature shifted toward pathways associated with extracellular matrix organization and tissue remodeling, marking the transition to a reparative and remodeling phase.

We identified five miRNAs (miR-181a-2-3p, miR-181a-5p, miR-221-5p, miR-342-5p, and miR-483-3p) that were consistently downregulated in EA patients both preoperatively and postoperatively compared with healthy controls. Functional enrichment analysis revealed that the predicted target genes of these five miRNAs were primarily involved in epigenetic regulation, muscle development, mitophagy, and metabolic pathways. A genetic study of isolated EA using genome-wide copy number variant analysis independently

identified significant enrichment of gene sets related to histone modification and cardiomyocyte differentiation, implicating genetic variation in myocardial development pathways as a key etiological factor in EA [34]. Together, our miRNA data and this genetic evidence support a potential synergistic role for epigenetic dysregulation and abnormal myocardial development in EA pathogenesis. Furthermore, an integrated miRNA-mRNA expression profiling study in EA patients similarly revealed gene regulatory networks involved in cardiac development, muscle function, and metabolic processes [22], complementing our findings.

Among the five persistently downregulated miRNAs, miR-483-3p demonstrated the strongest individual discriminatory power (AUC = 0.85). Previous studies have shown that miR-483-3p is involved in myocardial injury [35,36] and is associated with right ventricular remodeling and filling pressures in dilated cardiomyopathy [37]. These findings support our results and suggest that miR-483-3p may play a key regulatory role in myocardial adaptation and remodeling in EA. We further developed a multi-miRNA logistic regression model incorporating miR-483-3p, miR-192-5p, miR-532-5p, and miR-16-2-3p. This combined model showed excellent discriminative performance in LOOCV (AUC = 0.99), markedly outperforming any single miRNA. However, given the limited sample size, this model is susceptible to overfitting despite the use of LOOCV for internal validation, and its diagnostic value requires rigorous validation in larger, independent cohorts.

Time-series clustering of differentially expressed exosomal miRNAs revealed five distinct temporal patterns (C1–C5) that delineate a hierarchical molecular cascade associated with acute stress responses, structural remodeling and functional recovery following CR. In the immediate postoperative phase, Cluster C1 (initial upregulation followed by decline) may represent an early adaptive response regulating structural integrity and inflammatory resolution, while Cluster C2 (progressive upregulation) reflected heightened bioenergetic demands for cellular proliferation and regeneration. Cluster C3 (initial decline followed by upregulation) indicated tissue repair through intracellular signaling networks and immune regulation. Notably, Cluster C4 (sustained decline) was uniquely enriched in neuronal development signatures. This finding aligns with recent evidence of transcriptional dysregulation within cardiac neurons of congenital heart disease patients [38], suggesting a potential molecular link to the poorly understood neuro-cardiac crosstalk after congenital heart surgery. Most prominently, Cluster C5 (early rise then plateau) exhibited pronounced enrichment in embryonic organ development and core morphogenetic pathways such as Wnt and Notch signaling. This striking enrichment suggests that the CR procedure may reactivate fundamental embryonic programs, thereby driving long-term structural and functional restoration of the heart.

Our study identified that miR-224-5p, miR-548as-5p, and miR-30c-5p were consistently correlated with RV-FAC changes in both the acute and mid-term postoperative periods. Among these, miR-224-5p is closely associated with cardioprotective mechanisms, including the attenuation of oxidative stress and apoptosis in cardiomyocytes [39,40], as well as the improvement of endothelial function [41]. Similarly, miR-30c-5p plays a critical role in cardioprotection by alleviating myocardial ischemia-reperfusion injury [42,43] and promoting cardiac progenitor cell survival under pathological conditions [44]. Its clinical relevance is further supported by its correlation with the severity of acute coronary syndrome [45] and its potential as a heart failure biomarker [46]. Collectively, these findings suggest that miR-224-5p and miR-30c-5p are key regulators of cardiomyocyte survival, oxidative stress response, and endothelial function, supporting their potential utility as molecular markers and therapeutic targets in postoperative right ventricular functional recovery following CR.

NT-proBNP is a well-established biomarker of cardiac injury and myocardial stretch, and it has significant predictive value for postoperative adverse events in patients with congenital heart disease [47]. In our study, miR-338-3p showed significant correlations with NT-proBNP levels both preoperatively and in postoperative changes. miR-338-3p is implicated in myocardial fibrosis and ischemic injury [48,49].

Mechanistically, it exerts protective effects by inhibiting cardiac fibroblast activation [50] and mitigating cardiomyocyte injury through the regulation of apoptosis and inflammation [51]. Clinically, its expression levels in serum might be associated with the prognosis of dilated cardiomyopathy [50]. Building on previous reports, our findings indicate that miR-338-3p is closely associated with perioperative myocardial stress and may contribute to cardiac repair and functional recovery by modulating fibrosis, apoptosis, and inflammatory pathways, and thus holds potential for clinical monitoring and therapeutic intervention.

Despite several novel findings, this study has certain limitations. First, the sample size of 10 patients was relatively small. While this is considerable for rare disease research, it may still limit the stability and statistical power of the results. Future multicenter collaborations with larger cohorts are needed to validate these findings. Second, plasma exosomes originate from multiple cell types, making it difficult to ascertain whether the observed miRNA changes directly reflect cardiomyocyte-specific regulation. Future studies with paired myocardial tissue samples could help clarify this issue. Third, the observation time points were limited to within 7 days postoperatively. Longer-term molecular dynamics, such as changes at 1 month, 3 months, or even 1 year after surgery, remain unexplored. At the mechanistic level, this study primarily provides correlative evidence, and causal relationships require further functional validation. Moreover, this study focused on miRNAs, whereas integrative multi-omics analyses could provide a more comprehensive understanding. From a translational perspective, the potential therapeutic strategies suggested by our findings are worth exploring. Previous studies have demonstrated that the injection of bone marrow-derived stem cells can enhance ventricular recovery after CR [52]. Furthermore, a study from the Shanghai University team developed an injectable hydrogel system encapsulating miR-222-engineered extracellular vesicles, providing a feasible technical reference [53]. Finally, personalized therapy may represent a future research direction. Investigating whether preoperative exosomal miRNAs profiles can predict individual responses to CR could pave the way toward truly personalized treatment strategies.

5 Conclusions

To our knowledge, this study provides the first comprehensive characterization of the dynamic plasma exosomal miRNA landscape in patients with EA undergoing CR. Distinct miRNA signatures were identified before and after surgery, which may reflect a temporally coordinated molecular cascade involving acute stress responses, metabolic activation, and structural remodeling. On postoperative day 1, the cardiac-specific miRNAs miR-208a-3p, miR-208b-3p, and miR-499a-5p were markedly upregulated, reflecting surgery-related myocardial stress and early protective responses. By postoperative day 7, miRNAs associated with tissue repair and remodeling became predominant, indicating the transition toward structural recovery. Moreover, miR-224-5p, miR-548as-5p, and miR-30c-5p were significantly correlated with postoperative changes in right ventricular function, while miR-338-3p was closely associated with dynamic NT-proBNP levels, suggesting their potential as predictive biomarkers for postoperative recovery. In addition, a subset of persistently dysregulated miRNAs was identified, which may reflect the core pathological mechanisms of EA. Collectively, these findings provide new biological insights into the pathophysiology of EA and the postoperative repair process, highlighting the potential of exosomal miRNAs as prognostic biomarkers and therapeutic targets after CR.

Acknowledgement: We express our gratitude to all participants who volunteered for this study, as well as the hospital staff for facilitating the study.

Funding Statement: The authors declare that financial support was received for the research and/or publication of this article. This research was funded by the E Fund Congenital Heart Disease Medical Talent Cultivation and

Education Fund (grant number [2023QT0009]) and the Guangzhou Municipal Science and Technology Project (grant number [2023B03J1255]).

Author Contributions: The authors confirm contribution to the paper as follows: Conceptualization, Shusheng Wen; methodology, Jiaxiong Wu; software, Jing Ling; formal analysis, Jiaxiong Wu; investigation, Runzhang Liang and Naijimuding Abudurexiti; resources, Jiaxiong Wu, Runzhang Liang and Naijimuding Abudurexiti; data curation, Jiaxiong Wu, Runzhang Liang and Naijimuding Abudurexiti; writing—original draft preparation, Jiaxiong Wu; writing—review and editing, Shusheng Wen; visualization, Zirui Peng, Jinxin Li, Canxin Wang and Yong Zhang; supervision, Haiyun Yuan and Shusheng Wen; project administration, Haiyun Yuan and Shusheng Wen; funding acquisition, Shusheng Wen. All authors reviewed and approved the final version of the manuscript.

Availability of Data and Materials: The data that support the findings of this study are available from the corresponding authors upon reasonable request.

Ethics Approval: This study was approved by the Medical Ethics Committee of Guangdong Provincial People's Hospital (Approval No. KY2024-888-01) and was conducted in accordance with the principles of the Declaration of Helsinki. Written informed consent was obtained from all participants involved in the study.

Conflicts of Interest: The authors declare no conflicts of interest.

Supplementary Materials: The supplementary material is available online at https://www.techscience.com/doi/10.32604/schd.2026.077455/s1.

Abbreviations

EA	Ebstein's anomaly
CR	Cone reconstruction
miRNA/miRNAs	microRNA/microRNAs
DEMs	differentially expressed miRNAs
GO	Gene Ontology
KEGG	Kyoto Encyclopedia of Genes and Genomes
RV-FAC	right ventricular fractional area change
ROC	Receiver Operating Characteristic
AUC	Area Under the Curve
LOOCV	Leave-one-out cross-validation
NT-proBNP	N-terminal pro-B-type natriuretic peptide

References

1. Rydzewska K, Sylwestrzak O, Krekora M, Słodki M, Respondek-Liberska M. Ebstein's anomaly: epidemiological analysis and presentation of different prenatal management. J Matern Fetal Neonatal Med. 2022;35(17):3297–304. [CrossRef].
2. Singh DP, Hussain K, Horenstein MS, Mahajan K. Ebstein anomaly and malformation. In: StatPearls. Treasure Island, FL, USA: StatPearls Publishing; 2026.
3. Possner M, Gensini FJ, Mauchley DC, Krieger EV, Steinberg ZL. Ebstein's anomaly of the tricuspid valve: an overview of pathology and management. Curr Cardiol Rep. 2020;22(12):157. [CrossRef].
4. Holst KA, Connolly HM, Dearani JA. Ebstein's anomaly. Methodist Debakey Cardiovasc J. 2019;15(2):138–44. [CrossRef].
5. Flores Arizmendi A, Fernández Pineda L, Quero Jiménez C, Maître Azcárate MJ, Herráiz Sarachaga I, Urroz E, et al. The clinical profile of Ebstein's malformation as seen from the fetus to the adult in 52 patients. Cardiol Young. 2004;14(1):55–63. [CrossRef].
6. Sainathan S, da Fonseca da Silva L, da Silva JP. Ebstein's anomaly: contemporary management strategies. J Thorac Dis. 2020;12(3):1161–73. [CrossRef].

7. da Silva JP, Baumgratz JF, da Fonseca L, Franchi SM, Lopes LM, Tavares GMP, et al. The cone reconstruction of the tricuspid valve in Ebstein's anomaly. The operation: early and midterm results. J Thorac Cardiovasc Surg. 2007;133(1):215–23. [CrossRef].
8. Expert Consensus Panel, Chai P, Konstantinov IE, da Fonseca da Silva L, Qureshi M, Wackel P, et al. The american association for thoracic surgery (AATS) 2025 expert consensus document: management of ebstein anomaly in children and adults. J Thorac Cardiovasc Surg. 2025;170(1):1–16. [CrossRef].
9. Holst KA, Dearani JA, Said S, Pike RB, Connolly HM, Cannon BC, et al. Improving results of surgery for ebstein anomaly: where are we after 235 cone repairs? Ann Thorac Surg. 2018;105(1):160–8. [CrossRef].
10. Neijenhuis RML, Tsang VT, Marek J, Issitt R, Bonello B, Von Klemperer K, et al. Cone reconstruction for ebstein anomaly: late biventricular function and possible remodeling. J Thorac Cardiovasc Surg. 2021;161(3):1097–108. [CrossRef].
11. Welsh JA, Goberdhan DCI, O'Driscoll L, Buzas EI, Blenkiron C, Bussolati B, et al. Minimal information for studies of extracellular vesicles (MISEV2023): from basic to advanced approaches. J Extracell Vesicles. 2024;13(2):e12404. [CrossRef].
12. Tang Z, Feng S, Xiao Z. Progress on application of exosomes on cardiovascular disease: a ten-year retrospective analysis. Curr Probl Cardiol. 2026;51(3):103211. [CrossRef].
13. Li L, Zheng Z, Lan W, Tang N, Zhang D, Ling J, et al. Role of exosomes in cardiovascular disease: a key regulator of intercellular communication in cardiomyocytes. ACS Omega. 2025;10(18):18145–69. [CrossRef].
14. Zhang X, Sun S, Ren G, Liu W, Chen H. Advances in intercellular communication mediated by exosomal ncRNAs in cardiovascular disease. Int J Mol Sci. 2023;24(22):16197. [CrossRef].
15. Li H, Zhang J, Tan M, Yin Y, Song Y, Zhao Y, et al. Exosomes based strategies for cardiovascular diseases: opportunities and challenges. Biomaterials. 2024;308:122544. [CrossRef].
16. Bartel DP. microRNAs: genomics, biogenesis, mechanism, and function. Cell. 2004;116(2):281–97. [CrossRef].
17. Bartel DP. Metazoan microRNAs. Cell. 2018;173(1):20–51. [CrossRef].
18. Shang R, Lee S, Senavirathne G, Lai EC. microRNAs in action: biogenesis, function and regulation. Nat Rev Genet. 2023;24(12):816–33. [CrossRef].
19. Kozik A, Piotrowski M, Karpierz JI, Kowalewski M, Batko J. The Hidden Regulators: microRNAs in pediatric heart development and disease. J Clin Med. 2025;14(19):6833. [CrossRef].
20. Mannarino S, Calcaterra V, Puricelli F, Cecconi G, Chillemi C, Raso I, et al. The role of miRNA expression in congenital heart disease: insights into the mechanisms and biomarker potential. Child. 2025;12(5):611. [CrossRef].
21. González-Moyotl N, Huesca-Gómez C, Torres-Paz YE, Fuentevilla-Álvarez G, Romero-Maldonado S, Sámano R, et al. Paediatrics congenital heart disease is associated with plasma miRNAs. Pediatr Res. 2024;96(5):1220–7. [CrossRef].
22. Abu-Halima M, Wagner V, Becker LS, Ayesh BM, Abd El-Rahman M, Fischer U, et al. Integrated microRNA and mRNA expression profiling identifies novel targets and networks associated with Ebstein's anomaly. Cells. 2021;10(5):1066. [CrossRef].
23. Wei R, Zhao L, Kong G, Liu X, Zhu S, Zhang S, et al. Combination of size-exclusion chromatography and ultracentrifugation improves the proteomic profiling of plasma-derived small extracellular vesicles. Biol Proced Online. 2020;22:12. [CrossRef].
24. Betel D, Wilson M, Gabow A, Marks DS, Sander C. The microRNA.org resource: targets and expression. Nucleic Acids Res. 2008;36:D149–53. [CrossRef].
25. Rehmsmeier M, Steffen P, Hochsmann M, Giegerich R. Fast and effective prediction of microRNA/target duplexes. RNA. 2004;10(10):1507–17. [CrossRef].
26. Yu X, Zhao Y, Wang Q, Jiang X, Zhang L. MiR-150-5p attenuates heart failure by targeting MMP14 to regulate vascular smooth muscle cell function. Mol Cell Biochem. 2026;481(1):431–9. [CrossRef].
27. Liu M, Wang L, Liu Z, Liu D, Li T, Ding L, et al. MiR-222-3p loaded stem cell nanovesicles repair myocardial ischemia damage via inhibiting mitochondrial oxidative stress. Life Sci. 2025;365:123447. [CrossRef].
28. Zhang L, Yang J, Guo M, Hao M. MiR-223-3p affects myocardial inflammation and apoptosis following myocardial infarction via targeting FBXW7. J Thorac Dis. 2022;14(4):1146–56. [CrossRef].
29. Zhao X, Wang Y, Sun X. The functions of microRNA-208 in the heart. Diabetes Res Clin Pract. 2020;160:108004. [CrossRef].

30. Han J, Leppik L, Sztulman L, De Rosa R, Pfeiffer V, Busse L-C, et al. Dual roles of plasma miRNAs in myocardial injuries after polytrauma: miR-122-5p and miR-885-5p reflect inflammatory response, while miR-499a-5p and miR-194-5p contribute to cardiomyocyte damage. Cells. 2025;14(4):300. [CrossRef].
31. Sun H, Wang X, Pratt RE, Dzau VJ, Hodgkinson CP. C166 EVs potentiate miR cardiac reprogramming via miR-148a-3p. J Mol Cell Cardiol. 2024;190:48–61. [CrossRef].
32. McMullan E, Joladarashi D, Kishore R. Unpacking exosomes: a therapeutic frontier for cardiac repair. Curr Cardiol Rep. 2025;27(1):73. [CrossRef].
33. Neves KB, Rios FJ, Sevilla-Montero J, Montezano AC, Touyz RM. Exosomes and the cardiovascular system: role in cardiovascular health and disease. J Physiol. 2023;601(22):4923–36. [CrossRef].
34. Sicko RJ, Browne ML, Rigler SL, Druschel CM, Liu G, Fan R, et al. Genetic variants in isolated ebstein anomaly implicated in myocardial development pathways. PLoS One. 2016;11(10):e0165174. [CrossRef].
35. Saddic LA, Chang T-W, Sigurdsson MI, Heydarpour M, Raby BA, Shernan SK, et al. Integrated microRNA and mRNA responses to acute human left ventricular ischemia. Physiol Genomics. 2015;47(10):455–62. [CrossRef].
36. Sun H, Cai J, Xu L, Liu J, Chen M, Zheng M, et al. miR-483-3p regulates acute myocardial infarction by transcriptionally repressing insulin growth factor 1 expression. Mol Med Rep. 2018;17(3):4785–90. [CrossRef].
37. Gallo A, Agnese V, Sciacca S, Scardulla C, Cipriani M, Pilato M, et al. microRNA-30d and -483-3p for bi-ventricular remodelling and miR-126-3p for pulmonary hypertension in advanced heart failure. ESC Heart Fail. 2024;11(1):155–66. [CrossRef].
38. Thakur A, Kishore R. Neuro-genomic mapping of cardiac neurons with systemic analysis reveals cognitive and neurodevelopmental impacts in congenital heart disease. Life. 2025;15(9):1400. [CrossRef].
39. Mao C-Y, Zhang T-T, Li D-J, Zhou E, Fan Y-Q, He Q, et al. Extracellular vesicles from hypoxia-preconditioned mesenchymal stem cells alleviates myocardial injury by targeting thioredoxin-interacting protein-mediated hypoxia-inducible factor-1α pathway. World J Stem Cells. 2022;14(2):183–99. [CrossRef].
40. Liang G, Tang H, Guo C, Zhang M. miR-224-5p overexpression inhibits oxidative stress by regulating the PI3K/Akt/FoxO1 axis to attenuate hypoxia/reoxygenation-induced cardiomyocyte injury. J South Med Univ. 2024;44(6):1173–81. [CrossRef].
41. Zou X, Liu T, Huang Z, Zhou W, Yuan M, Zhao H, et al. SOX17 is a Critical Factor in Maintaining Endothelial Function in Pulmonary Hypertension by an Exosome-Mediated Autocrine Manner. Adv Sci. 2023;10(14):e2206139. [CrossRef].
42. Sun M, Guo M, Ma G, Zhang N, Pan F, Fan X, et al. microRNA-30c-5p protects against myocardial ischemia/reperfusion injury via regulation of Bach1/Nrf2. Toxicol Appl Pharmacol. 2021;426:115637. [CrossRef].
43. Wang L, Chen X, Wang Y, Zhao L, Zhao X, Wang Y. MiR-30c-5p mediates the effects of panax notoginseng saponins in myocardial ischemia reperfusion injury by inhibiting oxidative stress-induced cell damage. Biomed Pharmacother. 2020;125:109963. [CrossRef].
44. Purvis N, Kumari S, Chandrasekera D, Bellae Papannarao J, Gandhi S, van Hout I, et al. Diabetes induces dysregulation of microRNAs associated with survival, proliferation and self-renewal in cardiac progenitor cells. Diabetologia. 2021;64(6):1422–35. [CrossRef].
45. Chang B, Zhang X, Fang R, Li H, Zhou Y, Wang Y. Downregulation of serum miR-30c-5p serves as a biomarker to predict disease onset and short-term prognosis in acute coronary syndrome patients. J Cardiothorac Surg. 2025;20(1):12. [CrossRef].
46. Parvan R, Hosseinpour M, Moradi Y, Devaux Y, Cataliotti A, da Silva GJJ. Diagnostic performance of microRNAs in the detection of heart failure with reduced or preserved ejection fraction: a systematic review and meta-analysis. Eur J Heart Fail. 2022;24(12):2212–25. [CrossRef].
47. Shen H, He Q, Shao X, Lin Y-H, Wu D, Ma K, et al. Predictive value of NT-proBNP and hs-TnT for outcomes after pediatric congenital cardiac surgery. Int J Surg. 2024;110(6):3365–72. [CrossRef].
48. Fu D-L, Jiang H, Li C-Y, Gao T, Liu M-R, Li H-W. microRNA-338 in MSCs-derived exosomes inhibits cardiomyocyte apoptosis in myocardial infarction. Eur Rev Med Pharmacol Sci. 2020;24(19):10107–17. [CrossRef].
49. Wei Z, Lu Y, Qian C, Li J, Li X. Circ_0079480 facilitates proliferation, migration and fibrosis of atrial fibroblasts in atrial fibrillation by sponing miR-338-3p to activate the THBS1/TGF-β1/Smad3 signaling. Int J Cardiol. 2024;416:132486. [CrossRef].

50. Huang C, Wang R, Lu J, He Y, Wu Y, Ma W, et al. microRNA-338-3p as a therapeutic target in cardiac fibrosis through FGFR2 suppression. J Clin Lab Anal. 2022;36(8):e24584. [CrossRef].
51. Lin L, Wang L, Li A, Li Y, Gu X. CircDiaph3 aggravates H/R-induced cardiomyocyte apoptosis and inflammation through miR-338-3p/SRSF1 axis. J Bioenerg Biomembr. 2024;56(3):235–45. [CrossRef].
52. O'Leary PW, Qureshi MY, Cetta F, Nelson TJ, Holst KA, Dearani JA, et al. Cone reconstruction for ebstein anomaly: ventricular remodeling and preliminary impact of stem cell therapy. Mayo Clin Proc. 2021;96(12):3053–61. [CrossRef].
53. Wang Y, Meng D, Shi X, Hou Y, Zang S, Chen L, et al. Injectable hydrogel with miR-222-engineered extracellular vesicles ameliorates myocardial ischemic reperfusion injury via mechanotransduction. Cell Rep Med. 2025;6(3):101987. [CrossRef].